Proceedings of the 2006 WSEAS/IASME International Conference on Fluid Mechanics, Miami, Florida, USA, January 18-20, 2006 (pp31-39)

# Modified Hydro-Thermo-Diffusive Theory of Laminar Counterflow Premixed Flames

SIAVASH H. SOHRAB
Robert McCormick School of Engineering and Applied Science
Department of Mechanical Engineering
Northwestern University, Evanston, Illinois 60208
UNITED STATES OF AMERICA

*Abstract:* - Scale-invariant forms of conservation equations in reactive fields are discussed. The modified forms of the conservation equations at eddy-dynamic, and cluster-dynamic scales are then solved to describe the hydro-thermo-diffusive structure of laminar counterflow premixed flames. The predicted temperature profiles as well as the flame thermal thicknesses are found to be in good agreement with the measurements made on lean methane-air premixed flames stabilized on a stagnation-point burner at different stretch rates reported in a previous study. The error-function type geometry of the predicted temperature profile is also in accordance with the modified hydro-thermo-diffusive theory of laminar flames introduced earlier.

*Key-Words*: - Theory of laminar flames. Counterflow premixed flame. Laminar flame structure.

## 1 Introduction

The universality of turbulent phenomena from stochastic quantum fields to classical hydrodynamic fields resulted in recent introduction of a scale-invariant model of statistical mechanics and its application to the field of thermodynamics [4]. In the classical kinetic theory of gas by *Maxwell* and *Boltzmann*, particles are treated as point-mass singularities without any spatial extent. However, it is known that in reality molecules and atoms are not point-mass singularities but rather finite-size stable composite structures made of many smaller more elementary particles. Therefore, the fact that the classical approach of assuming point-mass entities has been successful in the description of molecular dynamics suggests that this same approach could be generalized to macroscopic scales.

Following such guidelines, a scale-invariant model of statistical mechanics for equilibrium fields of eddy-, cluster-, molecular-, atomic-dynamics corresponding to the scales $\beta =$ e, c, m, a, schematically shown in Fig.1 was introduced [4] and applied to the derivation of the invariant forms of conservation equations [5] and the introduction of a modified hydro-thermo-diffusive theory of laminar flame [6]. In the present study, the invariant forms of the conservation equations are employed to investigate the hydro-thermo-diffusive structure of laminar counterflow premixed flames.

The predicted temperature and velocity profiles as well as the laminar flame thickness are shown to be in accordance with the experimental measurements.

## 2 Scale-Invariant Forms of the Conservation Equations for Reactive Fields

Following the classical methods [1-3], the invariant definitions of the density $\rho_\beta$, and the velocity of *atom* $\mathbf{u}_\beta$, *element* $\mathbf{v}_\beta$, and *system* $\mathbf{w}_\beta$ at the scale $\beta$ are given as [4]

$$\rho_\beta = n_\beta m_\beta = m_\beta \int f_\beta du_\beta \quad , \qquad \mathbf{u}_\beta = \mathbf{v}_{\beta-1} \qquad (1)$$

$$\mathbf{v}_\beta = \rho_\beta^{-1} m_\beta \int \mathbf{u}_\beta f_\beta d\mathbf{u}_\beta \quad , \qquad \mathbf{w}_\beta = \mathbf{v}_{\beta+1} \qquad (2)$$

Also, the invariant definitions of the peculiar and the diffusion velocities are given as [4]

$$\mathbf{V}'_\beta = \mathbf{u}_\beta - \mathbf{v}_\beta \quad , \qquad \mathbf{V}_\beta = \mathbf{v}_\beta - \mathbf{w}_\beta = \mathbf{V}'_{\beta+1} \qquad (3)$$

Next, following the classical methods [1-3], the scale-invariant forms of mass, thermal energy, and linear momentum conservation equations at scale $\beta$ are given as [5, 6]

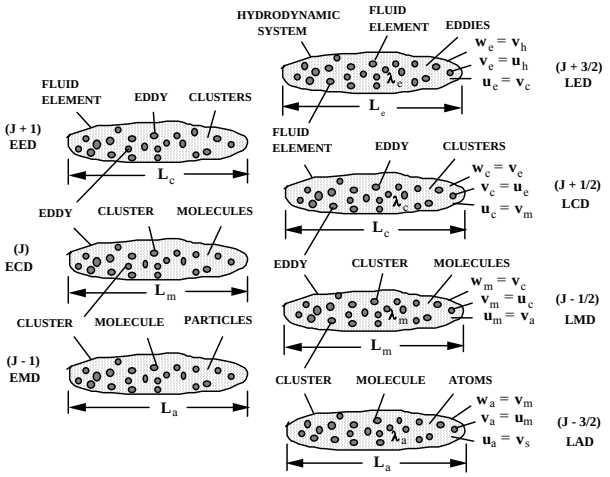


**Fig.1 Hierarchy of statistical fields for equilibrium eddy-, cluster-, and molecular-dynamic scales and the associated laminar flow fields.**

$$\frac{\partial \rho_\beta}{\partial t} + \nabla.\left(\rho_\beta \mathbf{v}_\beta\right) = \Omega_\beta \qquad (4)$$

$$\frac{\partial \varepsilon_\beta}{\partial t} + \nabla.\left(\varepsilon_\beta \mathbf{v}_\beta\right) = 0 \qquad (5)$$

$$\frac{\partial \mathbf{p}_\beta}{\partial t} + \nabla.\left(\mathbf{p}_\beta \mathbf{v}_\beta\right) = 0 \qquad (6)$$

involving the *volumetric density* of thermal energy $\varepsilon_\beta = \rho_\beta h_\beta$ and linear momentum $\mathbf{p}_\beta = \rho_\beta \mathbf{v}_\beta$. Also, $\Omega_\beta$ is the chemical reaction rate and $h_\beta$ is the absolute enthalpy.

The local velocity $\mathbf{v}_\beta$ in (4)-(6) is expressed in terms of the convective $\mathbf{w}_\beta$ and the diffusive $\mathbf{V}_\beta$ velocities [5]

$$\mathbf{v}_\beta = \mathbf{w}_\beta + \mathbf{V}_{\beta g} \quad , \quad \mathbf{V}_{\beta g} = -D_\beta \nabla \ln(\rho_\beta) \qquad (7a)$$

$$\mathbf{v}_\beta = \mathbf{w}_\beta + \mathbf{V}_{\beta tg} \quad , \quad \mathbf{V}_{\beta tg} = -\alpha_\beta \nabla \ln(\varepsilon_\beta) \qquad (7b)$$

$$\mathbf{v}_\beta = \mathbf{w}_\beta + \mathbf{V}_{\beta hg} \quad , \quad \mathbf{V}_{\beta hg} = -\nu_\beta \nabla \ln(\mathbf{p}_\beta) \qquad (7c)$$

where ($\mathbf{V}_{\beta g}$, $\mathbf{V}_{\beta tg}$, $\mathbf{V}_{\beta hg}$) are respectively the diffusive, the thermo-diffusive, the linear hydro-diffusive velocities.

Substitutions from (7a)-(7c) into (4)-(6), neglecting cross-diffusion terms and assuming constant transport coefficients with $Sc_\beta = Pr_\beta = 1$, result in [5, 6]

$$\frac{\partial \rho_\beta}{\partial t} + \mathbf{w}_\beta.\nabla \rho_\beta - D_\beta \nabla^2 \rho_\beta = \Omega_\beta \qquad (8)$$

$$\frac{\partial T_\beta}{\partial t} + \mathbf{w}_\beta.\nabla T_\beta - \alpha_\beta \nabla^2 T_\beta = -h_\beta \Omega_\beta / (\rho_\beta c_{p\beta}) \qquad (9)$$

$$\frac{\partial \mathbf{v}_\beta}{\partial t} + \mathbf{w}_\beta.\nabla \mathbf{v}_\beta - \nu_\beta \nabla^2 \mathbf{v}_\beta = -\mathbf{v}_\beta \Omega_\beta / \rho_\beta \qquad (10)$$

An important feature of the modified equation of motion (10) is that it involves a convective velocity $\mathbf{w}_\beta$ that is different from the local fluid velocity $\mathbf{v}_\beta$.

## 4 Symmetric Counterflow Laminar Premixed Flames

The importance of combustion in stagnation-point or counterflow burning configurations to the modeling of strained flamelets in turbulent combustion is well recognized [3, 7-21]. Therefore, the objective of the present study is to understand the structure of two identical laminar premixed flames in axi-symmetric counterflow as shown in Fig.2.

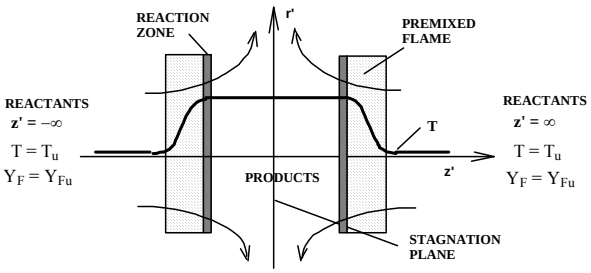


**Fig.2 Schematic drawing of axi-symmetric counterflow premixed flames.**

For cylindrically symmetric counterflows, the *steady* forms of (8)-(10) under the assumption $\partial(\theta,\ y)/\partial r' \approx 0$ become [6, 22]

$$w'_z \frac{dy}{dz'} = D \frac{d^2 y}{dz'^2} - \Lambda y e^{\beta(\theta-1)} \delta(z'_f) \qquad (11)$$

$$w'_z \frac{d\theta}{dz'} = \alpha \frac{d^2 \theta}{dz'^2} + \Lambda y e^{\beta(\theta-1)} \delta(z'_f) \qquad (12)$$

$$w'_r \frac{\partial v}{\partial r'} + w'_z \frac{\partial v}{\partial z'} = \nu \frac{\partial^2 v}{\partial z'^2} + v \Lambda y e^{\beta(\theta-1)} \delta(z'_f) \qquad (13)$$

The velocities $\mathbf{w}$ and $\mathbf{v}$ are respectively the convective and the local velocity and $(z', r')$ are the axial and the radial coordinates. The following dimensionless parameters have been defined

$\theta = (T - T_u)/(T_b - T_u)$ , $y = Y_F/Y_{Fu}$,

$$\rho = \rho_{Fu} = \rho Y_{Fu} \quad , \quad \Lambda \equiv (\nu_F W_F B/\rho)\, e^{-\beta/\chi} \qquad (14)$$

The adiabatic flame temperature $T_b$, the *Zeldovich* number $\beta$, and the coefficient of thermal expansion $\chi$ are

$$T_b = T_u + QY_{Fu}/\nu_F W_F c_p$$

$$\beta = E(T_b - T_u)/RT_b^2 \quad , \quad \chi = (T_b - T_u)/T_b \qquad (15)$$

and one assumes that $\beta >> 1$. Also, unity *Prandtl* Pr = $\nu/\alpha$, *Schmidt* Sc = $\nu/D$, and *Lewis* Le = $\alpha/D$ numbers are assumed, such that $\theta$, y, and v fields will be similar under identical boundary conditions.

## 5 Solution of the Modified Equation of Motion for Axi-symmetric Stagnation-point and Counterflow

The solution of the modified equation of motion for the classical problems of laminar axi-symmetric stagnation-point flow and counterflow jets were discussed in a previous study [22]. It was shown that the solution within a thin boundary layer next to the wall should be determined at LCD scale with the relevant lengths ($l_c = 10^{-7}$, $\lambda_c = 10^{-5}$, $L_c = 10^{-3}$) m. The convective velocity field $(w'_{rc}, w'_{zc})$ outside of the boundary layer is expressed as

$$w'_{rc} = \Gamma_c r' \quad , \quad w'_{zc} = -2\Gamma_c z' \qquad (16)$$

involving the velocity gradient $\Gamma_c = \Gamma/\sqrt{\pi}$ with $\Gamma$ defined in (23). The subscript (c) refers to the laminar cluster-dynamic (LCD) scale $\beta$ = c and the relevant kinematic viscosity for this scale is $\nu_c = l_c u_c/3 = \lambda_m v_m/3$ [5]. Under the additional boundary layer assumption $\partial v_{rc}/\partial r' \ll \partial v_{rc}/\partial z'$, and with introduction of the dimensionless velocities

$$(\mathbf{v_{rc}}, \mathbf{v_{zc}}, \mathbf{w}_{zc}) = (\mathbf{v'_{rc}}, \mathbf{v'_{zc}}, \mathbf{w'}_{zc})/\sqrt{\nu_c \Gamma_c} \qquad (17)$$

and coordinates

$$\xi_c = r'/\delta_c \quad , \quad \zeta_c = z'/\delta_c \quad , \quad \delta_c = \sqrt{\nu_c/\Gamma_c} \qquad (18)$$

the solution of the steady form of (4) and the r-component of (10) in the absence of chemical reactions $\Omega$ = 0 can be expressed in terms of the stream function [22]

$$\Psi_c = -\xi_c^2 \int_0^{\zeta_c} \mathrm{erf}(y)dy \qquad (19)$$

that leads to the velocity components

$$v_{rc} = -\frac{1}{\xi_c}\frac{\partial \Psi_c}{\partial \zeta_c} = \xi_c \mathrm{erf}(\zeta_c) \qquad (20)$$

$$v_{zc} = \frac{1}{\xi_c}\frac{\partial \Psi_c}{\partial \xi_c} = -2\int_0^{\zeta_c} \mathrm{erf}(y)dy \qquad (21)$$

The velocity profiles calculated from (20) and (21) are shown in Fig.3 for the range $0 < \zeta_c < 2$.

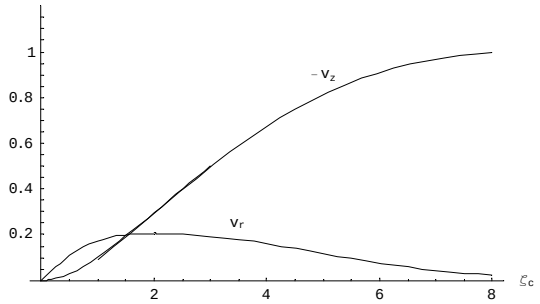


**Fig.3 Laminar axi-symmetric stagnation-point flow inside and outside of the boundary layer [22].**

The flow field outside of the thin boundary layer must be determined at the next larger scale of LED with the relevant "atomic", element, and system velocities ($\mathbf{u}_e$, $\mathbf{v}_e$, $\mathbf{w}_e$) and the associated length scales ($l_e = 10^{-5}$, $\lambda_e = 10^{-3}$, $L_e = 10^{-1}$) m. The convective velocity for outer flow is known and given by [2]

$$w'_{re} = \Gamma r' \quad , \quad w'_{ze} = -2\Gamma z' \qquad (22)$$

where $\Gamma$ is defined as the ratio of the jet velocity at the nozzles $w'_{zo}$ and the separation distance between the nozzles L (Fig.3)

$$\Gamma = w'_{zeo}/L \qquad (23)$$

The solutions of (8) and (10) that satisfy the boundary conditions and match the inner solutions at the edge of the boundary layer were presented earlier [22] and the resulting calculated velocity profiles that match the solutions within the boundary layer are also shown in Fig.3 in the range $2 < \zeta_c < 8$.

The hydrodynamic problem that is more relevant to the present study is that of two axi-symmetric counterflow finite jets shown in Fig.2. The solution of the steady form of (4) and the z-component of (10) with the additional assumptions that $\partial v_{ze}/\partial r' = 0$ and that the thickness of the inner free viscous layer at LCD scale is negligible, under the appropriate boundary conditions results in the stream function [22]

$$\Psi_e = -\frac{\xi_e^2}{2}\mathrm{erf}(\zeta_e) \qquad (24)$$

leading to the velocities

$$v_{ze} = -\mathrm{erf}(\zeta_e) \tag{25}$$

$$v_{re} = \frac{\xi_e}{\sqrt{\pi}} \exp(-\zeta_e^2) \tag{26}$$

where $\zeta_e = z'/\delta_e$ and $\delta_e = \sqrt{\nu_e / \Gamma}$. The axial and radial velocity profiles calculated from (25)-(26) are shown in Fig.4 and are in qualitative agreement with experimental observations in Fig.8 of *Tsuji* and *Yamaoka* [16].

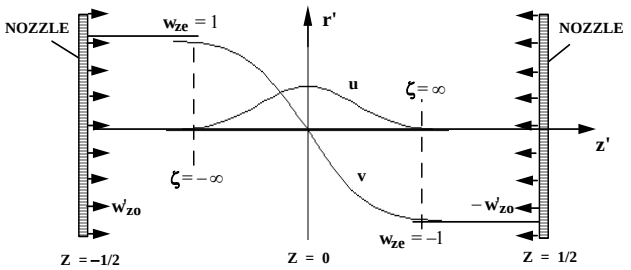


**Fig.4 Calculated velocity profiles for axi-symmetric finite-jet counterflow ($u = v_{re}$, $v = v_{ze}$) from (25)-(26).**

Some of the streamlines calculated from (24) are shown in Fig.5.

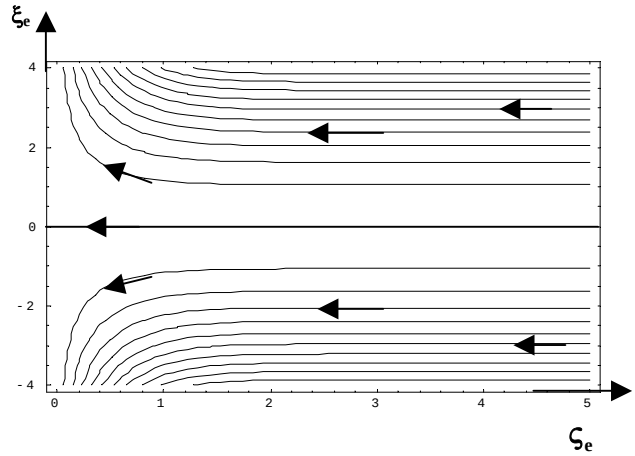


**Fig.5 Calculated streamlines from (24) for outer LED scale of axi-symmetric finite-jet counterflow.**

According to (24), the jets do not diverge until they reach the position of the hydrodynamic "boundary layer" at $\zeta_e = 2.4$ that corresponds to the inner scale $\zeta_c \to \infty$. Hence, two axi-symmetric opposing jets of infinite radial extent that are infinitely far from each other will retain their one-dimensional axial flow for a very long distance (Fig.5) and only begin to diverge as they arrive near the stagnation plane as is to be expected.

The thickness of the hydrodynamic "boundary layer" at LED scale is obtained from the solution (25) as the location $\zeta_e = 2.4$ where $v_{ze} = 0.9995$ such that

$$\delta_H \approx 2.4 \frac{L}{\sqrt{\mathrm{Re}}} = 2.4\sqrt{\frac{\nu}{\Gamma}} \tag{27}$$

in exact agreement with the classical result [2]. For typical values L = 5 cm, $w'_{zo}$ = 50 cm/s, $\nu_c$ = 0.16 cm$^2$/s leading to Re = 1563, one obtains $\delta_H$ = 3.0 mm from (27). However, according to (25) the edge of the boundary layer has already been reached to an accuracy of 0.995 at the shorter distance of $\zeta_e \approx 2$ such that $\delta_H \approx 2\delta_e$.

## 6. Hydro-Thermo-Diffusive Structure of Counterflow Premixed Flames

Next, the hydro-thermo-diffusive structure of symmetric premixed flames stabilization within the counterflow jets shown in Fig.3 is examined. The behavior of the flames will depend on the relative magnitude of the jet axial velocity at infinity $w'_{zo}$ versus the laminar flame propagation velocity $v'_f$. One can identify four distinguishable burning regimes listed below

**(a) When $w'_{zo} = 0$ two free-propagating flames propagate at the velocity $v'_p = v'_f$ towards $z' \to \pm\infty$ without experiencing any stretch.**

**(b) When $w'_{zo} < -v'_f$ two flames propagate at the reduced velocity $v'_p = v'_f - w'_{zo}$ towards $z' \to \pm\infty$ without experiencing any stretch.**

**(c) When $w'_{zo} = -(v'_f + \varepsilon)$ and $\varepsilon << 1$ two flames become stationary at $z'_f = \pm\delta_H$ without experiencing any stretch.**

**(d) When $w'_{zo} > -v'_f$ two flames are stationary at $z'_f < \pm\delta_H$ and experience finite stretch.**

Cases (a) and (b) above would lead to flame flash-back if one considers finite-jet counterflow burners with nozzle exits at z' = ± L/2.

The above considerations suggest a close correspondence between free-propagating laminar premixed flames on the one hand, and burner-stabilized counterflow premixed flames on the other hand. In particular, the case (c) corresponds to the classical stationary planar laminar premixed flame that does not experience any stretching effects.

### 6.1 Far-Field Convective Coordinate

Next, the hydrodynamic velocity field at LED scale for a reactive counterflow is considered. At this

scale, the flame will appear as a mathematical surface of discontinuity located at the position $z'_f$ given by

$$v'_f + v'_b/2 = -w'_z = 2\Gamma z'_f \tag{35}$$

where $v'_f$ is the laminar flame propagation velocity. The velocity jump $v'_b$ across the flame is related to the laminar flame propagation velocity $v'_f$ by the mass balance across the flame sheet $\rho_b(v'_f + v'_b) = \rho_u v'_f$. The temperature, mass fraction of deficient component, and the velocity profiles on either side of the flame sheet are obtained from the solution of (11)-(13) with $\partial v_{ze}/\partial r' = 0$ as

$$\theta = 1 - y = 1 \qquad \zeta < \zeta_f \tag{36}$$

$$\theta = 1 - y = 0 \qquad \zeta > \zeta_f \tag{37}$$

and

$$v_{ze} = -(v_f + v_b)\frac{\mathrm{erf}(\zeta)}{\mathrm{erf}(\zeta_f)} \qquad 0 < \zeta < \zeta_f \tag{38}$$

$$v_{ze} = -v_f + (v_f + w_o)\frac{\mathrm{erf}(\zeta) - \mathrm{erf}(\zeta_f)}{1 - \mathrm{erf}(\zeta_f)} \quad \zeta_f < \zeta < \infty \tag{39}$$

where $\zeta = z'/\delta_e$ and $\delta_e = \sqrt{\nu/\Gamma}$. The radial velocity can be obtained from (4) and (38)-(39). The schematic diagram of calculated velocity profiles for reactive flow at LED scale are shown in Fig.6.

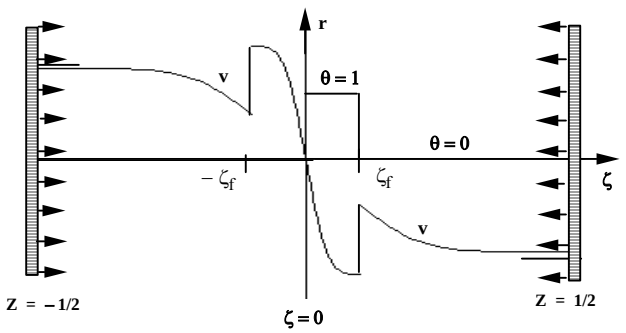


**Fig.6 Calculated velocity profile for reactive axi-symmetric counter flow at LED scale ($v = v_{ze}$).**

The temperature profile as seen at this same scale is shown in Fig.6, but only for the half-plane $\zeta > 0$.

### 6.2 Outer Convective-Diffusive Coordinate

To reveal the hydro-thermo-diffusive structure of the flame, one moves to the smaller scale of laminar cluster dynamics LCD (Fig.1) with the characteristic velocities ($\mathbf{u_c}$, $\mathbf{v_c}$, $\mathbf{w_c}$) and the associated length scales ($l_c = 10^{-7}$, $\lambda_c = 10^{-5}$, $L_c = 10^{-3}$) m. For simplicity, unity *Prandtl*, *Schmidt*, and *Lewis* numbers will be assumed, $\nu = \alpha = D$.

In the neighborhood of the flame sheet at $z'_f$ (25) gives

$$v_{ze} \approx -2(\zeta - \zeta_f)/\sqrt{\pi} \tag{40}$$

or

$$v'_{ze} \approx -2\Gamma(z' - z'_f)/\sqrt{\pi} \tag{41}$$

In a previous study [22], it was shown that the appropriate scaling factor between LED and LCD fields was ¼. Similarly, for the analysis of hydro-thermo-diffusive flame structure, one introduces the stretched coordinate

$$\eta = z'/\sqrt{\nu/\Gamma_c} = z'/\delta_c \tag{42}$$

with the characteristic length $\delta_c = \delta_e/4$. Under the assumption $\nu_c = \nu_e$, this coordinate stretching is equivalent to a factor of 16 increase of the stretch rate $\Gamma_c = 16\Gamma$. By (41) and the identity $w'_c = v'_e$, the convective velocity in the flame structure is given as

$$w'_{zc} = -32\Gamma(z' - z'_f) \tag{43}$$

By substitutions from (42)-(43) into (11)-(13) and noting the assumptions $\nu = \alpha = D$ and $\partial v_{zc}/\partial r = 0$ one obtains

$$\frac{d^2y}{d\eta^2} + 2(\eta - \eta_f)\frac{dy}{d\eta} = \frac{\Lambda}{16\Gamma} y e^{\beta(\theta-1)}\delta(\eta_r) \tag{44}$$

$$\frac{d^2\theta}{d\eta^2} + 2(\eta - \eta_f)\frac{d\theta}{dx} = -\frac{\Lambda}{16\Gamma} y e^{\beta(\theta-1)}\delta(\eta_r) \tag{45}$$

$$\frac{d^2v_{zc}}{d\eta^2} + 2(\eta - \eta_f)\frac{dv_{zc}}{dx} = -v_{zc}\frac{\Lambda}{16\Gamma} y e^{\beta(\theta-1)}\delta(\eta_r) \tag{46}$$

that must satisfy the boundary conditions

$$\begin{aligned} &\eta \to \infty && \theta = y - 1 = v + 1 = 0 \\ &\eta = \eta_f && \theta - 1/2 = y - 1/2 = v_{zc} + 1 + v_b/2 = 0 \\ &\eta \to -\infty && \theta - 1 = y = v_{zc} + 1 + v_b = 0 \end{aligned} \tag{47}$$

It is important to note that the delta functions associated with the reaction terms in (44)-(46) have now been moved from the position of the flame $\zeta_f$ in (11)-(13) of the far field coordinate (Fig.6) to the position of the reaction zone $\eta_r$ of the thermo-diffusive coordinate $\eta$ (Fig.7).

The solutions of the system (44)-(46) outside of the thin reaction zone where $\Lambda = 0$ and subject to the boundary conditions (47) are

$$\theta = 1 - y = \frac{1}{2}\,\mathrm{erfc}(\eta - \eta_f) \tag{48}$$

$$v_{zc} = -v_f - \frac{v_b}{2}\,\mathrm{erfc}(\eta - \eta_f) \tag{49}$$

The schematic diagram of the calculated hydrodynamic flame structure is shown in Fig.7.

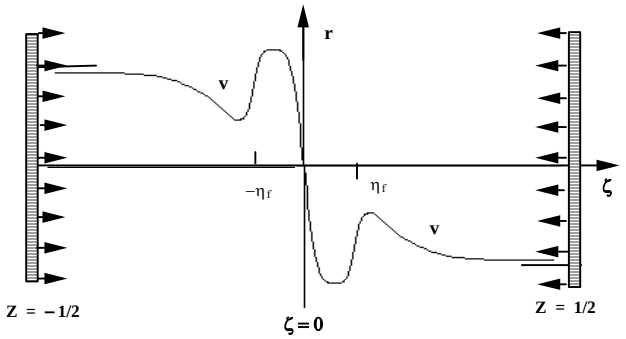


**Fig.7 Calculated velocity profile for reactive axi-symmetric counter flow at LCD scale ($v = v_{zc}$)**

It is noted that the calculated velocity profile in Fig.7 is not based on actual physico-chemical properties. The exact relation between the inner thermo-diffusive coordinate $\eta$ at LCD scale and the outer hydrodynamic coordinate $\zeta$ at the LED scale was discussed earlier [22].

### 6.3 Inner Reactive-Diffusive Coordinate

The analysis of the much thinner reaction zone that is embedded within the hydro-thermo-diffusive zone follows the classical methods [3, 7-10, 23] as described in an earlier study [6]. Since the reaction zone thickness is about $4l_T/\beta = \delta_f/\beta$ and the *Zeldovich* number $\beta$ defined in (21) is large, under the present model the analysis of the reaction zone requires moving to the next smaller scale of laminar-molecular dynamics LMD (Figs.1, 2) with the characteristic velocities ($\mathbf{u}_m$, $\mathbf{v}_m$, $\mathbf{w}_m$) and the associated length scales ($l_m = 10^{-9}$, $\lambda_m = 10^{-7}$, $L_m = 10^{-5}$) m. From the analysis of reaction zone according to the modified theory of laminar flames the flame propagation velocity was obtained as [6]

$$v_f'^2 = \frac{8\pi\nu_F\rho_b\rho_O\alpha B'}{(\rho_u - \rho_b)W_O\beta^2}\,e^{-\beta/\chi}\exp(2\zeta_i^2) \tag{50}$$

For realistic physico-chemical properties, a flame speed of $v'_f = 42.1$ cm/s was calculated from (50) for one-step stoichiometric combustion of methane-air [6] in close agreement with the experimental observations [24-27]. The value of about $v'_f = 42$ cm/s has also been obtained in a number of numerical investigations using more complex multi-step kinetic models [28-30].

An important aspect of strained velocity fields (Fig.2) is their impact on flame patterns such as those caused by thermo-diffusive flame instabilities [3, 23, 31-33]. For example, the cellular premixed flame of rich butane-air in stagnation-point flow against a flat quartz plate at low stretch rates shown in Fig.8a is converted to a star-shaped flame [19, 34] shown in Fig.8b at higher rates of stretch. At still higher stretch rates the flame surface becomes smooth until its eventual extinction.

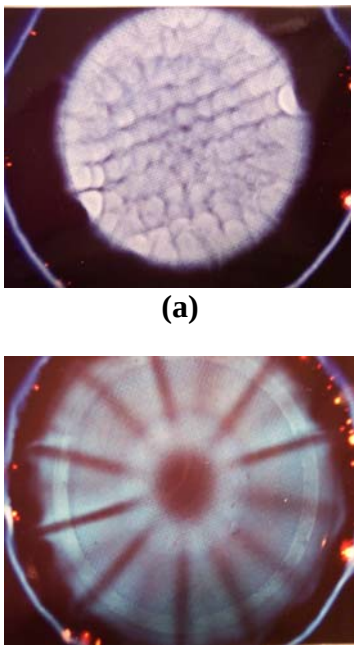

**(a)**

**(b)**

**Fig.8 Premixed flames of rich butane-air in stagnation-point flow against a flat quartz plate. (a) cellular flame (b) star-shaped flame.**

The symmetry apparent between the modified forms of the conservation equations (8)-(10) could help in the future development of theories on hydro-thermo-diffusive instabilities of laminar flames.

## 7. Comparisons with Measured Flame Thermal Thickness and Temperature Profiles

The temperature profiles of lean methane-air flames measured at constant equivalence ratio of $\phi = 0.8$ in the stagnation-point flow against the flat surface of a quartz plate from an earlier investigation [35] for the

nozzle velocities $w'_{zo}$ = (30, 50, 70) cm/s and nozzle rim to plate spacing L/2 = 1.26 cm are shown in Fig.9. The measured flame temperature will be somewhat reduced due to downstream heat loss to the quartz plate. It is also noted that even with symmetric counterflow premixed flames, because of the radiant heat loss one cannot achieve truly adiabatic premixed flames [36, 37].

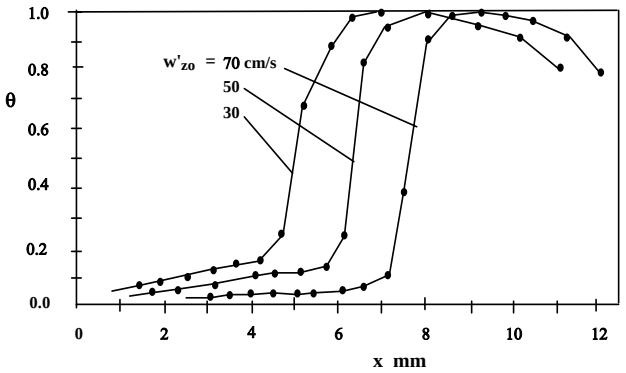


**Fig.9 Measured temperature profiles for methane-air premixed flames in stagnation-point flow with ϕ = 0.8, L = 1.26 cm, x = z′, and $w'_{zo}$ = (30, 50, 70) cm/s [35].**

The data in Fig.9 are similar to the temperature profiles reported in an earlier study [38]. For velocities below 70 cm/s, the gas leaving the burner is above ambient temperature of 300 K, thus complicating the evaluation of the flame thickness. Since thermocouple wire tends to slightly "drag" the flame along with it, the measured flame thicknesses are expected to be slightly larger than the actual ones. From the temperature profiles in Fig.9 the flame thermal thicknesses of about (3.0, 2.5, 2.0) mm are estimated for the nozzle velocities $w'_{zo}$ = (30, 50, 70) cm/s.

According to the solution (48) the upstream and downstream edges of the flame to an accuracy of 0.995 will be respectively at $(\eta_+ - \eta_f) = 2$ and $(\eta_- - \eta_f) = -2$ such that the predicted flame thickness becomes $(\eta_+ - \eta_-) = 4$ that by (42) gives

$$\delta_f = \sqrt{\nu / \Gamma} \qquad (51)$$

For the measured flame temperature of 1500 K [35] and the average temperature of 900 K the thermal diffusivity of air is about $\varepsilon \approx \nu \approx 1.4$ cm$^2$/s. Also, since the experiments [35] involve stagnation-point flow rather than counter flow, with an estimated boundary layer thickness of 2.5 mm from (27) the burner distance becomes $1.26 - 2.5 \approx 1$ cm that gives the nozzle separation distance of L = 2 cm. Hence, the nozzle velocities $w'_{zeo}$ = (30, 50, 70) cm/s will give by (23) the stretch rates $\Gamma = (15,\ 25,\ 35)\ s^{-1}$ such that the predicted flame thermal thicknesses calculated from (51) become $\delta_f = (3.0,\ 2.4,\ 2.0)$ mm in good agreement with the measure values (3.0, 2.5, 2.0) mm estimated from Fig.9.

The predicted temperature profile (48) has error-function type geometry as schematically shown in Fig.10a in accordance with the data in Fig.9.

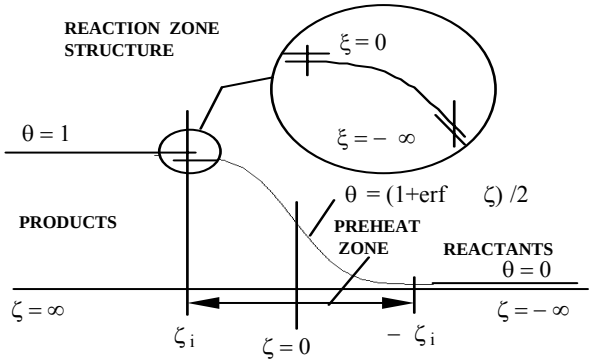


**Fig.10a Flame structure according to the modified theory of laminar flames [6].**

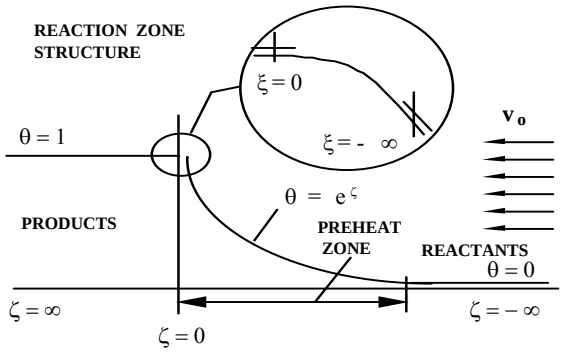


**Fig.10b Flame structure according to the classical theory of laminar flames.**

To facilitate the comparisons, the temperature profile according to the classical theory of laminar flame is schematically shown in Fig.10b. As the stretch rate is reduced, the temperature profiles of stretched flames become increasingly similar to those of un-stretched laminar flames. Hence, it is expect that temperature profiles of free propagating laminar flames also have error-function type geometry in accordance with the modified theory of laminar flames [6] and the measured temperature profiles in the literature [16, 25, 39-41] that are all similar to Fig.21 of *Lewis and von Elbe* [42].

Attention is next focused on the sign of the curvature of the temperature profile near the reaction zone in Fig.10a and the fact that the temperature in the reaction zone matches that in the preheat zone from above. By comparison, the sign of the curvature of temperature profile near the reaction zone according to the classical theory of laminar flames schematically shown in Fig.10b is opposite to that in Fig.10a. As a result, the temperature within the reaction zone must be matched to that in the preheat zone from below. However, this violates the fact that temperature in the reaction zone must be higher than that in the preheat zone.

According to Sec.6 when $w'_{zo} = -v'_f$ the weakly stretched flame will locate at $\delta_{He} \approx 2\delta_e$ and becomes equivalent to a freely propagating laminar flame corresponding to the case (c). Therefore, similar to the outer velocity field given in (28) one can express the convective velocity within the hydrodynamic structure of laminar flame as

$$w'_{zc} = -2\Gamma_f (z' - z'_f) \tag{52}$$

where $\Gamma_f$ is the self-induced flame stretch. For free propagating flames the axial velocity jump across the flame is $v'_b$. Therefore, with $\delta_{He} \approx 2\delta_e = 8\delta_c = 8\ell_T$ and the characteristic diffusion length defined as $\delta_c = \ell_T = \alpha / v'_f$, the stretch $\Gamma_f$ in (52) becomes

$$\Gamma_f = v'_b / 8\ell_T \tag{53}$$

Substituting from (52)-(53) and the new axial coordinate

$$\varsigma = z'\sqrt{v_b}\,/(2\sqrt{2}\ell_T) \tag{54}$$

where $v_b = v'_b / v'_f$ into (12) one obtains

$$\frac{d^2\theta}{d\varsigma^2} + 2(\varsigma - \varsigma_f)\frac{d\theta}{d\varsigma} = -\frac{8\Lambda\alpha}{v_b v'^2_f} y e^{\beta(\theta-1)} \delta(\varsigma_r) \tag{55}$$

The solution of (55) and (47) outside of the thin reaction zone where $\Lambda = 0$ is

$$\theta = 1 - y = \frac{1}{2}\,\mathrm{erfc}(\varsigma - \varsigma_f) \tag{56}$$

According to (56) the positions $(\varsigma_+ - \varsigma_f \approx 2,\ \varsigma_- - \varsigma_f \approx -2)$ respectively correspond to the upstream and the downstream edges of the flame thermal thickness to an accuracy of 0.995. Therefore, the predicted flame thermal thickness is $\varsigma_+ - \varsigma_- = 4$ that by (54) results in

$$\delta_f \approx 8\sqrt{2}(\alpha / \sqrt{v'_f v'_b}) \tag{57}$$

From the mass balance across the flame $\rho_b(v'_f + v'_b) = \rho_u v'_f$ and the ideal gas law under the assumption of constant pressure one obtains

$$v'_b = v'_f(\rho_u / \rho_b - 1) = v'_f(T_b / T_u - 1) \tag{58}$$

Therefore, for the typical average temperature ratio of $T_b/T_u$ = 5, one obtains from (58) the typical velocity ratio $v'_b \approx 4v'_f$ such that (57) becomes

$$\delta_f \approx \frac{8\sqrt{2}}{\sqrt{(T_b / T_u - 1)}}\frac{\alpha}{v'_f} \approx 4\sqrt{2}\ell_T \tag{59}$$

that is a factor of $2\sqrt{2}$ larger than the result reported by *Turns* [43]. The result (59) satisfies the required spatio-temporal invariance of a flame front propagating by diffusion $\delta_f = 4\sqrt{2\alpha t'}$ where $t' = \alpha / v'^2_f$. One notes that with $v'_b \approx 4v'_f$ the self-induced flame stretch (53) becomes $\Gamma_f = v'_f / 2\ell_T$. In view of (52), the apparent velocity gradient within the flame structure could be expressed as $\Gamma^*_f = v'_f / \ell_T$ such that

$$\delta_c = \sqrt{\nu / \Gamma^*_f} = \sqrt{\nu\alpha / v'^2_f} = \alpha / v'_f = \ell_T \tag{60}$$

For the methane-air premixed flame at $\phi$ = 0.8 the flame propagation velocity is about 30 cm/s [25]. Therefore, the temperature profile for $w'_{ZO}$ = 30 cm/s shown in Fig.9 is expected to be very close to the temperature profile of a free-propagating laminar premixed flame in the absence of stretch effects that corresponds to the case (c) identified in Sec.6 above. At $\phi$ = 0.8, at the mean adiabatic temperature of 1000 K, with $\alpha$ = 1.6 cm$^2$/s and $v'_f = 30$ cm/s the predicted laminar flame thickness from (59) is $\delta_f \approx 3.0$ mm in agreement with the data of Fig.9. In the study of *Eng et al* [41] for lean methane-air premixed flame at $\phi$ = 0.7 stabilized on a flat burner, the flame thermal thickness of about 3.0 mm was measured at the flame temperature of about 1600 K. Now, for the average temperature of 950 K, the thermal diffusivity of air is about $\alpha$ = 1.55 cm$^2$/s such that for the flame speed of $v'_f = 23$ cm/s at $\phi$ = 0.7 [25] the predicted flame thermal thickness becomes $\delta_f$ = 3.8 mm. However, at the lower average temperature of 800 K one gets for air $\alpha$ = 1.21 cm$^2$/s that leads to $\delta_f$ = 3.0 mm in close agreement with the observations [41]. In comparison to the result (59), the predicted flame thermal

thickness according to the classical theory of laminar flames is

$$\delta_f \approx \ell_T = \alpha / v_f' \qquad (61)$$

that in general will deviate from the experimental measurements by a factor of about $4\sqrt{2}$ .

## 8 Concluding Remarks

Scale-invariant forms of the conservation equations for energy, species mass fractions, and momentum in chemically reactive fields were employed to present a modified hydro-thermo-diffusive theory of laminar counterflow premixed flames. The predicted flame temperature profile and the flame thermal thickness were shown to be in accordance with the experimental measurements for lean methane-air premixed flames.

*Acknowledgements:*
This research was in part supported by NASA micro-gravity combustion science program under grant NAG3-1863.

*References:*

[1] de Groot, R. S., and Mazur, P., *Nonequilibrium Thermodynamics*, North-Holland, 1962.
[2] Schlichting, H., *Boundary-Layer Theory*, McGraw Hill, New York, 1968.
[3] Williams, F. A., *Combustion Theory*, 2nd Ed., Addison-Wesley, New York, 1985.
[4] Sohrab, S. H., *Rev. Gén. Therm.* **38**, 845 (1999).
[5] Sohrab, S. H., Transport phenomena and conservation equations for multi-component chemically reactive ideal gas mixtures. *Proceeding of the 31st ASME National Heat Transfer Conference*, HTD-Vol. **328**, 37-60 (1996).
[6] Sohrab, S. H., *WSEAS Transactions on Mathematics*, Issue 4, Vol.3, 755 (2004).
[7] Liñán, A., The asymptotic structure of counterflow diffusion flames for large activation energies. *Acta Astronautica* **1**, 1007 (1974).
[8] Peters, N., *Proc. Combust. Inst.* 20, p. 1231 (1986).
[9] Warnatz, J., Maas, U., and Dibble, R. W., *Combustion,* Springer, New York, 1996.
[10] Buckmaster, J. D., and Ludford, G. S. S., *Theory of Laminar Flames*, Cambridge University Press, Cambridge, 1982.
[11] Saitoh, T., and Otsuka, Y., *Combust. Sci. Technol.* **12**, 135 (1976).
[12] Daneshyar, H., Mendes-Lopes, J. M. C., and Ludford, G. S. S., *Proc. Combust. Inst.* 19, p. 413 (1982).
[13] Seshadri, K., *Int. J. Engin. Sci.* **21**, 103 (1983).
[14] Stahl, G., and Warnatz, J., *Combust. Flame* **85**, 285 (1991).
[15] Sohrab, S. H., Ye, Z. Y., Law, C. K., *Combust. Sci. Technol.* **45**, 27 (1986).
[16] Yamaoka, I., and Tsuji, H., *Proc. Combust. Inst.* 17, p. 843 (1978).
[17] Tsuji, H., and Yamaoka, I., *Proc. Combust. Inst.* 19, p. 1533 (1982).
[18] Tsuji, H., and Yamaoka, I., *Proc. Combust. Inst.* 20, p. 1883 (1984).
[19] Ishizuka, S., and Law, C. K., *Proc. Combust. Inst.* 19, p. 327 (1982).
[20] Sato, J., *Proc. Combust. Inst.* 19, p.1541 (1982).
[21] Wu, C. K., and Law, C. K., *Proc. Combust. Inst.* 20, p. 1941 (1984).
[22] Sohrab, S. H., *IASME Transactions*. Issue **7**, Vol.2, 1097 (2005).
[23] Joulin, G., and Clavin, P., *Combust. Flame* **35**, 139 (1979).
[24] Günther, R., and Janisch, G., *Combust. Flame* **19**, 49 (1972).
[25] Andrews, G. E., and Bradley, D., *Combust. Flame* **19**, 275 (1972); **20**, 77 (1973).
[26] Lindow, R., *Brennstoff Wärme Kraft* **20**:8 (1968).
[27] Reed, S. B., Mineur, J., and McNaughton, J. P., *J. Inst. Fuel* **44**, 149 (1971).
[28] Smoot, D. L., Hecker, W. C., and Williams, G. A., *Combust. Flame* **26**, 323 (1976).
[29] Tsatsaronis, G., *Combust. Flame* **33**:217 (1978).
[30] Chen, C. L., and Sohrab, S. H., *Combust. Flame* **101**, 360 (1995).
[31] Clavin, P., *Prog. Energy Combust. Sci.* **11**, 1 (1985).
[32] Zeldovich, Y. B., Barenblatt, G. I., Librovich, V. B., and Makhviladze, G. M., *The Mathematical Theory of Combustion and Explosion*, Moscow: Nauka, 1980.
[33] Sivashinsky, G. I., *Annual Review of Fluid Mechanics* **15**, 179 (1983).
[34] Lee, H, and Sohrab, S. H., *Eastern States Section Meeting*, The Combustion Institute, October 16-18, 1995, Worcester Polytechnic Institute, Worcester, MA.
[35] Kurz, O., and Sohrab, S. H., *First Joint Western-Central-Eastern States Section Meeting*, The Combustion Institute, March 14-17, 1999, George Washington University, Washington DC.
[36] Liu, G. E., Ye, Z. Y., and Sohrab, S. H., *Combust. Flame* **64**, 193-201 (1986).
[37] Sohrab, S. H., and Law, C. K., *Int. J. Heat Mass Transfer* **27**, 291 (1984).
[38] Chen, Z. H., Lin, T. H., and Sohrab, S. H., *Combust. Sci. Technol.* **60**, 63 (1988).
[39] Fristrom, R. M., Grunfelder, C., and Favin, J., *J. Phys. Chem.* **64**, 1386 (1960).
[40] Ferguson, R. C., and Keck, C. J., *Combust. Flame* **34**, 85 (1979).
[41] Eng, J. A., Zhu, D. L., and Law, C. K., *Combust. Flame* **100**, 645 (1995).
[42] Lewis B., and von Elbe, G., *Combustion Flame and Explosion of Gases*, Academic Press, New York (1987).
[43] Turns, R. S., *An Introduction to Combustion,* McGraw Hill, New York, 1996, p.221.